Contribution of a Single-Turn α-Helix to the Conformational Stability and Activity of the Alkaline Proteinase Inhibitor of *Pseudomonas aeruginosa*

Robert D. Gray*,‡,§ and John O. Trent‡,⊥

Departments of Biochemistry & Molecular Biology, Medicine, and Ophthalmology & Visual Sciences and the James Graham Brown Cancer Center, University of Louisville School of Medicine, Louisville, Kentucky 40292

Received August 9, 2004; Revised Manuscript Received November 27, 2004

ABSTRACT: The alkaline proteinase inhibitor of *Pseudomonas aeruginosa* (APRin), a high-affinity inhibitor of the serralysin family of bacterial metalloproteinases, is folded into an eight-stranded β-barrel with an N-terminal trunk linked to the barrel by a single-turn α-helix (helix A, residues 8−11). We show here that deletion or modification of helix A decreases the conformational stability of APRin as assessed by thermal and chemical denaturation with guanidinium chloride (GdmCl). The apparent melting temperature T_m of the wild-type protein was 81.5 °C at pH 7.1 as assessed by circular dichroism and 87.5 °C by differential scanning calorimetry. Reduction of the single disulfide bond of APRin decreased T_m by ∼18 °C, while deletion of residues 6−10 or 1−10 lowered T_m by ∼8 and ∼14 °C, respectively. ΔG_u as assessed by chemical denaturation was 7.2 kcal mol^{-1} at 25 °C for wild-type APRin and was decreased by 3.4, 2.4, and 2.6 kcal mol^{-1} by disulfide reduction, deletion of residues 6−10, and deletion of residues 1−10, respectively. In contrast, deletion of residues 1−5 had no significant effect on either T_m or ΔG_u. Substitution of five helix-breaking Gly or Pro residues in positions 6−10 as well as disruption of hydrogen bonds involving residues within helix A (mutants Asp10Pro and Trp15Phe) also decreased T_m and ΔG_u. The data suggest that a hydrogen-bonding network involving Leu11 in helix A and Trp15 located at the top of the barrel may prevent access of solvent to the interior of the barrel. Disruption of the helix could facilitate solvation of the nonpolar interior of the barrel, thereby destabilizing its folded structure. Kinetic studies with single amino acid mutants in helix A indicate that it modulates the affinity of APRin for APR primarily by influencing the dissociation rate of the inhibitor from the complex.

The Gram-negative bacteria *Pseudomonas aeruginosa*, *Serratia marcescens*, and *Erwinia chrysanthemi* are each capable of secreting 50 kDa zinc-dependent endopeptidases into the extracellular environment. These enzymes have been classified within the serralysin branch of the metzincin superfamily of metalloproteinases (*1*). The metzincin family, named for a conserved Met residue located in a turn near the base of the zinc binding site, also includes the matrix metalloproteinases, the reprolysins, and the adamalysins (*2*). Alkaline proteinase (APR),[1] the serralysin homologue of *P. aeruginosa*, was first purified by Morihara (*3*) from the culture medium of this organism. It is capable of degrading a variety of human proteins including γ-interferon (*4*) and laminin (*5*), as well as proteolytically activating matrix metalloproteinases (*6*−*8*) and Hageman factor (*9*).

Serralysin-secreting bacteria are also capable of producing serralysin-specific inhibitors. These proteins of approximately 11.5 kDa mass are found in the periplasmic space, where they are thought to protect the organism from adventitious proteolysis during proteinase secretion (*10*). To date, seven homologous inhibitors from *Pseudomonas*, *Serratia*, and *Erwinia* species have been recognized through genomic analysis (*11*).

Crystal structures of two different serralysin−inhibitor complexes show that the inhibitors from *P. aeruginosa* (*11*) and *E. chrysanthemi* (*12*) are both folded into eight-stranded β barrels with an N-terminal peptide of five residues that protrudes from the barrel and occupies the carboxyl side of the substrate binding site of the enzyme (Figure 1, left panel). In the complex with the pseudomonal proteins, the α-amino group of the N-terminal residue of the inhibitor and its carbonyl oxygen were shown to chelate the catalytic zinc (*11*). Additional interactions between the enzyme and inhibitor involve inhibitor β strands IV and V and their connecting loops, which contact the proteinase near its Met turn. The crystal structures of the two enzyme−inhibitor complexes also reveal that the inhibitor residues 1−7 are appended to the β-barrel by a single-turn α-helix (helix A) composed of residues 8−11. The panel on the right in Figure 1 shows a detailed view of the network of hydrogen bonds in the APR−APRin complex that stabilizes the helical conformation. These interactions (summarized in Table 1) involve the

* To whom correspondence should be addressed at the Department of Biochemistry & Molecular Biology, University of Louisville, Louisville, KY 40292. Telephone 502-852-5226; fax 502-852-6222; e-mail rdgray@louisville.edu.

‡ Department of Biochemistry & Molecular Biology.

§ Department of Ophthalmology & Visual Sciences.

⊥ Department of Medicine and James Graham Brown Cancer Center.

[1] Abbreviations: APR, alkaline proteinase from *P. aeruginosa* (E.C. 3.4.24.40); aprin, alkaline proteinase inhibitor from *P. aeruginosa*; CD, circular dichroism; $\Delta(1-n)$ APRin, APRin with residues 1 through *n* deleted; DSC, differential scanning calorimetry; DTT, dithiothreitol; GdmCl, guanidinium chloride; SDS−PAGE, sodium dodecyl sufate−polyacrylamide gel electrophoresis; T_m, thermal transition midpoint temperature; wt, wild type.

10.1021/bi048287q CCC: $30.25
Published on Web 01/25/2005

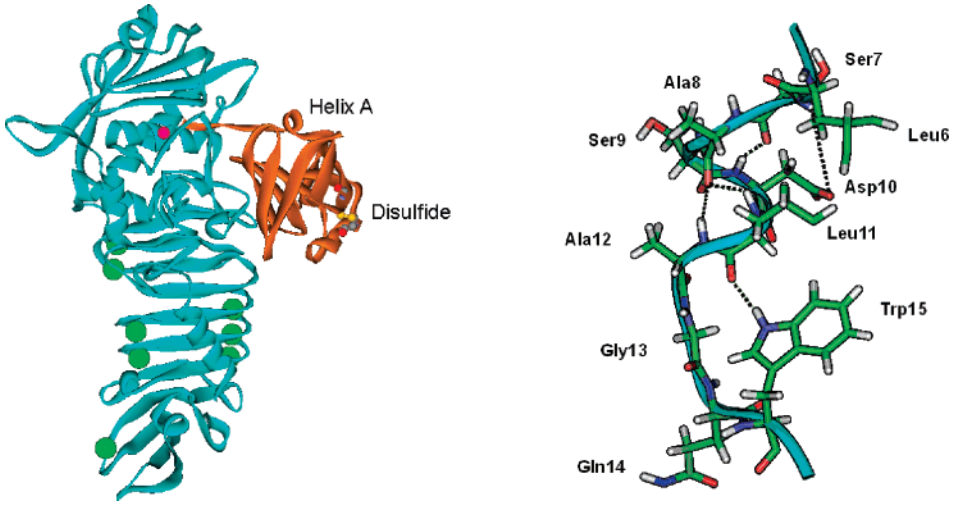

FIGURE 1: Ribbon diagram of the complex between wt APRin and APRin (left), showing the connection of the N-terminal trunk of APRin to the β-barrel by helix A, and the hydrogen-bonding network that stabilizes helix A (right). In the diagram on the left, alkaline proteinase (APR) is represented by the blue ribbons with the catalytic zinc shown as a red sphere; the green spheres represent calcium ions. The inhibitor APRin is represented by the brown ribbons. Helix A and the disulfide bond connecting Cys26 and Cys49 are identified. The diagram on the right shows a detailed representation of residues 7−15 that flank helix A (residues 8−11). The dotted lines illustrate hydrogen bonds involving residues in the helix (summarized in Table 1). The illustrations were generated by use of X-ray coordinates of the complex between APR and APRin in Protein Data Bank file 1JIW (*11*) in conjunction with software from Accelerys, Inc., San Diego, CA.

Table 1: Hydrogen Bonds in Helix A of APRin[a]

donor	acceptor	donor	acceptor
Ser7 NH	Asp10 $O^{\delta 2}$	Trp15 $NH^{\epsilon 1}$	Leu11 CO
Leu11 NH	Ala8 CO	Ala12 NH	Ala8 CO
Asp10 NH	Ser7 CO	Asp10 NH	Ser7 O^{γ}

[a] Hydrogen bonds were detected in the crystal structure of APRin from Protein Data Bank file 1JIW (*11*) with the program Insight II. The same bonding pattern was preserved in the model of free APRin generated by molecular dynamics simulation.

peptide bonds of Ser7, Ala8, Asp10, and Leu11, as well as side-chain groups of Ser7, Asp10, and Trp15.

We have shown that wt APRin inhibits APR with an apparent dissociation constant K_D of about 4 pM (*13*, *14*). In keeping with the role of the N-terminus of the inhibitor as revealed by crystallography, these studies showed that successive deletion of up to five residues from the N-terminus resulted in progressively decreased inhibitory potency, while deletion of six or more residues completely abolished inhibition. In addition, residues 6−10 were critically important for full inhibitory potency since the deletion mutant Δ(6−10) was inactive. Inhibition could be restored (but at a 100−200-fold increase in K_D) by substituting five Gly or Pro residues at positions 6−10. These studies showed not only that the length of the N-terminal trunk is functionally important but also that positions 6−10, which are not in direct contact with the proteinase, influence the strength of inhibition.

An obvious structural role for residues 6−10 could be related to the fact that three of these residues form the N-terminal part of a helix composed of residues 8−11. Thus a goal of the present study was to investigate the effect disrupting helix A on inhibition and on the conformational stability of APRin. A molecular dynamics simulation of the solvated inhibitor suggests that helix A is maintained in the absence of APR, a conclusion that we have recently validated by NMR studies that show definitively that it is present the proteinase-free inhibitor (*15*).

The results presented here show that residues 6−10, and by inference helix A, is a strong determinant of the overall conformational stability of the inhibitor as assessed by thermal and chemical denaturation. We propose that helix A and its associated hydrogen-bonding network prevents access of solvent to the highly hydrophobic interior of the β-barrel structure. In addition, analysis of kinetics of interaction of selected single-residue mutant inhibitors with APR indicates that helix A also influences the affinity of APRin for APR.

MATERIALS AND METHODS

Materials

Proteins. The recombinant APRin proteins were expressed in *Escherichia coli* strain BL21(DE3) (Novagen, Madison, WI) or BL21(DE3)-Star (Stratagene, La Jolla, CA) by use of the pET22b+ expression vector (Novagen) engineered to contain the coding sequence of the mature APRin protein from *P. aeruginosa*. The proteins were purified by chromatography as previously described (*13*). Expression plasmids encoding the APRin mutants Ala8Pro, Asp10Ala, Asp10Pro, and Trp15Phe were prepared by use of the QuikChange site-directed mutagenesis kit (Stratagene, San Diego, CA) with the wt APRin-pET22b+ vector as template. Mutagenic oligonucleotides in which the wt codon of interest was replaced with either the Pro codon CCG or the Phe codon TTT were purchased in gel-purified form from Integrated DNA Technologies, Coralville, IA. The APRin coding sequence of the mutants was verified by DNA sequence analysis of the expression plasmids, and the purity and mass of the recombinant proteins were verified by SDS−PAGE and electrospray mass spectrometry. The $(Cys)_2$ form of wt APRin was prepared immediately before use by reduction of the wt protein with 4 mM dithiothreitol in either 20 mM Na phosphate and 0.1 M NaCl, pH 7.1, or 50 mM Tris-HCl, pH 7.4.

Methods

Thermal Denaturation Assessed by CD Spectroscopy. Thermal denaturation experiments were carried out in 20 mM sodium phosphate and 0.1 M NaCl, pH 7.1. Phosphate buffer was used because its ionization enthalpy is close to zero, thus ensuring maintenance of a constant pH with changing temperature (*16*). CD spectra were recorded on a Jasco J-710 spectropolarimeter equipped with a NesLab programmable water bath. Four consecutive spectra were averaged. The scan rate was 5 nm/min, the response time was 16 s, and the bandwidth was 1 nm. Protein solutions (generally 5−10 μM) were initially warmed to 42 °C for 10−20 min for partial degassing and then transferred to a stoppered water-jacketed cuvette. A room-temperature reference spectrum was recorded from 240 to 190 nm. The sample was then heated to ∼40 °C and allowed to equilibrate for at least 5 min, after which the temperature was increased at a rate of 20 °C/h in 1 °C increments to a final value of 90−98 °C. After a 2-min equilibration period, the ellipticity at 230 nm (corresponding to the maximum signal change) was recorded at each temperature. Each reading is the average of six separate measurements spaced over a period of 2 min. At the conclusion of the thermal denaturation experiment, the sample was cooled to room temperature over a period of about 40 min and a final reference spectrum was recorded. A few experiments were also carried out with wt APRin and Δ(1−10) APRin at high protein concentration (∼100 μM) or faster scan rates (50 °C/h) to approximate conditions used in the calorimetric experiments described below. Essentially identical results were obtained in the CD experiments at high protein concentration and the faster scan rate.

Differential Scanning Calorimetry. The thermal stability of wt and Δ(1−10) APRin was also assessed by differential scanning calorimetry. These experiments were carried out by Dr. V. Fresca, MicroCal, Inc., Northhampton, MA, using a MicroCal VP-DSC instrument. Prior to the calorimetric measurements, the protein solutions (∼80 μM) were exhaustively dialyzed versus 20 mM sodium phosphate and 0.1 M NaCl, pH 7.1, followed by centrifugation, filtration, and degassing. Calorimetry was carried out at a pressure of ∼30 psi and a scan rate of 60 °C/h. Dialysis buffer was used as a blank.

GdmCl Denaturation. Chemical denaturation experiments were monitored by CD and carried out by titration of the protein samples in 50 mM Tris-HCl (pH 7.4) with 8.0 M GdmCl (ultrapure grade, Schwarz/Mann Biotech, Cleveland, OH) in the same buffer. The extent of unfolding was determined by recording the ellipticity of the sample in a 1-cm path length cuvette maintained at 25 °C; the experimental values were corrected for dilution by multiplying by the appropriate dilution factor. Reversibility of unfolding of wt APRin was demonstrated by titration of a sample of the GdmCl-denatured protein with denaturant-free buffer. Essentially identical values of ΔG_u and m were obtained for the folding and unfolding reactions.

Analysis of CD Unfolding Data. Denaturation of small single-domain proteins can often be described by a reversible two-state equilibrium between folded and unfolded proteins in which the equilibrium constant K_u is given by

$$K_u = f_u/(1 - f_u) \quad (1)$$

where f_u is the fraction of unfolded protein (*17*−*19*). The standard free energy of unfolding can therefore defined as

$$\Delta G^\circ = -RT \ln K_u \quad (2)$$

CD melting curves were analyzed routinely within the two-state framework to give T_m, the midpoint temperature of the transition, and ΔH_m, the van't Hoff enthalpy change, by using the algorithm of John and Weeks (*20*). In this method, which has the advantage of minimizing uncertainty in defining the pre- and post-melting baselines, the first derivative of ellipticity with respect to temperature ($d\theta/dT$) is fit to eq 3 by optimizing the values of the adjustable parameters ΔH_m, T_m, and a baseline correction factor A:

$$d\theta/dT = Af(1 - f)(T^2) \quad (3)$$

where $f = K/(K + 1)$ and $K = \exp[(\Delta H_m/R)(1/T_m - 1/T)]$. Values of $d\theta/dT$ were obtained by numerical differentiation of the experimental θ versus temperature curves with software supplied with the CD instrument. In a few instances, CD melting profiles were also analyzed by (*21*)

$$\theta = \{\theta_f + m_f T_m + (\theta_u + m_u T)\exp[(\Delta H_m/R)(1/T_m - 1/T)]\}/\{1 + \exp[(\Delta H_m/R)(1/T_m - 1/T)]\} \quad (4)$$

where θ_f, θ_u, m_f, and m_u are the intercepts and slopes of the pre- and post-transition baselines of the folded and unfolded states, respectively, with the other parameters defined above. Similar results were obtained with both methods of data analysis.

GdmCl denaturation curves were analyzed by the linear extrapolation approximation of the two-state model as described by Pace and Shaw (*22*). In this method, ΔG at any concentration of denaturant D is assumed to follow the relationship

$$\Delta G = \Delta G_u - m[D] \quad (5)$$

where ΔG is defined in eq 2, ΔG_u is the extrapolated conformational stability of the protein in the absence of denaturant, and [D] is the concentration of GdmCl. Optimized values of ΔG_u and m were obtained by fitting the ellipticity−denaturant profiles by nonlinear least squares to (*23*)

$$\theta = \{\theta_f + m_f[D] + (\theta_u + m_u[D])\exp(-(\Delta G_u - m[D]/RT))\}/\{1 + \exp(-(\Delta G_u - m[D]/RT))\} \quad (6)$$

In eq 6 θ_f, θ_u, m_f and m_u, the intercepts and slopes of the pre- and post-transition baselines of the folded and unfolded states, respectively, were adjusted along with m and ΔG_u to give an the best fit to the θ versus [D] data points. The nonlinear least squares module in the program Slide Write Plus 6.0 (Advanced Graphics Software, Encinitis, CA) was used to fit the CD data to eq 3, 4, or 6 as appropriate.

Analysis of DSC Data. The DSC melting profiles of wt and Δ(1−10) APRin were analyzed by use of the calorimeter manufacturer's software. Because both proteins exhibited an anomalous high-temperature baseline, it was not possible to determine ΔH and ΔC_p reliably; however, T_m could be determined from the maximum in the melting profiles.

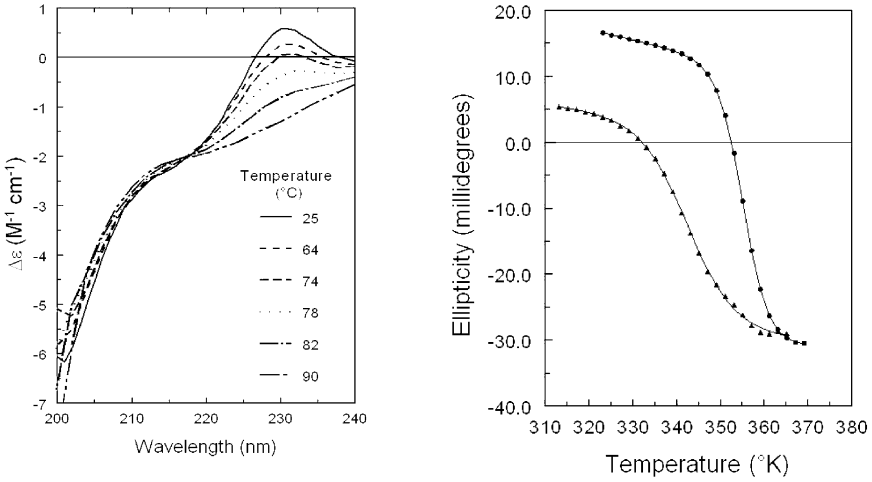

FIGURE 2: Thermal denaturation of wt APRin as assessed by CD spectroscopy. The left panel shows CD spectra of wt APRin (8.5 μM) in 20 mM sodium phosphate and 0.1 M NaCl, pH 7.1, at the indicated temperatures. The right panel shows thermal denaturation profiles at 230 nm of wt (●) and Δ(1−10) (▲) APRin determined at protein concentrations of 100 μM and path lengths of 0.1 cm. The lines show the least-squares best fit of the experimental points to eq 4 from which the optimized thermodynamic parameters are $\Delta H_m = 86.5 \pm 0.8$ kcal mol^{-1}, $T_m = 355.5 \pm 0.05$ (82.35 °C) for wt APRin and $\Delta H_m = 42.1 \pm 2.7$ kcal mol^{-1}, $T_m = 343.1 \pm 0.5$ °K (70 °C) for Δ(1−10) APRin.

Analysis of Inhibition Data. Association (k_{on}) and dissociation (k_{off}) rate constants for interaction of the Ala8Pro, Asp10Ala, Asp10Pro, and Trp15Phe mutant APRins with APR were determined as described previously (*13*) from the time dependence of development of inhibition by using the thiopeptolide Ac-Pro-Leu-Gly-[2-mercapto-4-methylpentanoyl]-Leu-Gly ethyl ester (Bachem, King of Prussia, PA) as substrate (*24*). The apparent equilibrium dissociation constant K_D was estimated from the ratio k_{off}/k_{on}.

Molecular Dynamics Simulations. Molecular dynamics simulations were carried out on a 32 processor SGI Origin 2000 as previously described for the complex between APRin and the catalytic domain of APR (*14*). The starting model of APRin was based on its coordinates in the crystal structure of the APR−APRin complex [Protein Data Bank entry 1JIW (*11*)]. The starting structure was hydrated in a 10 Å box of TIP3P waters by standard AMBER rules. Na^+ counterions were placed randomly for charge neutrality. Simulations were performed in the isothermal isobaric ensemble (300 K, 1 atm) with AMBER 7.0 and parm96.dat with periodic boundary conditions and the Particle-Mesh-Ewald algorithm. The simulations used the MPI version of the Sander routine (1.5 fs time step) with SHAKE to freeze all bonds involving hydrogen. Initial equilibrium for 155 ps following the general protocol of Trent (*25*) was performed with gradual heating and removal of positional restraints. Production runs were 1.5 ns in length. This time period was judged to be sufficient to observe relaxation of the helix to a different structure, and the system was stable in terms of total energy after the equilibrium period of 155 ps.

RESULTS

Thermal Unfolding Assessed by CD. Figure 2 (left panel) shows a family of CD spectra determined at various stages of thermal denaturation of wt APRin. The largest temperature-dependent change in ellipticity was at 230 nm, with smaller changes in ellipticity below 230 nm. A clear isodichroic point near 222 nm was present in the family of spectra, suggesting an equilibrium distribution between two species that contributed to the CD signal. Similar CD spectra with maxima at ∼230 nm were obtained for each of the mutant APRins in this study with the exception of the Trp15Phe mutant. In this protein, the peak at 230 nm was absent, with $\theta_{230} \approx 0$. Consequently, the change in θ_{230} was about two-thirds of the signal observed for proteins that contained Trp15. Prominent CD bands at ∼230 nm have been observed with other small proteins of low helix content and have been assigned either to Trp or Tyr chromophores, depending upon the particular protein (*26*).

The reversibility of the thermal denaturation process was assessed by monitoring the recovery of the CD spectrum after the heated protein was returned to room temperature. The extent of refolding depended both on the highest temperature and on the rate of recooling. For example, wt APRin heated to 98 °C and cooled to room temperature over approximately 1 h recovered ∼75% of the original CD signal at 230 nm, suggesting that ∼25% of the protein was irreversibly unfolded under these conditions. However, when the wt protein was heated to a temperature at which only ∼95% was unfolded and then returned to room temperature within 10−15 min, >95% of θ_{230} was recovered, showing that the extent of irreversibility was time-dependent. There was no visible precipitate after heating any of the proteins used in these studies; in addition, ∼100% of the 280 nm absorbance was recovered after centrifugation of a heated sample of wt APRin. To assess the possibility that heating induced covalent changes in wt APRin, a heat-denatured sample was subjected to electrospray mass spectrometry. No change in protein mass was detected, thereby ruling out a major heat-induced change in covalent structure. However, the precision of the measurements was not sufficient to detect a relatively small change in mass such deamidation of Asn or Gln.

CD melting profiles for wt APRin and an N-terminal truncation mutant in which residues 1−10 were deleted [Δ(1−10) APRin] are shown in the right panel of Figure 2. These data were analyzed with eq 4 to generate apparent T_m and ΔH_m values; excellent fits were obtained for both proteins as illustrated by the solid lines in the figure, which represent the calculated melting curves from the optimized T_m and ΔH_m values. For the pair of experiments shown in

Table 2: Thermodynamic Parameters for the Denaturation of Wild-Type and Mutant APRins and the Kinetic and Binding Constants for Their Interaction with APR[a]

	N-terminal sequence	T_m (°C)	ΔH_m (kcal mol^{-1})	ΔG_u (kcal mol^{-1})	$k_{on} \times 10^{-3}$ (M^{-1} s^{-1})	$k_{off} \times 10^{6}$ (s^{-1})	K_D (pM)
wt	SSLILLSASDLA-	81.5 ± 0.8	76.6 ± 4.4	7.2	290 ± 60	1.15 ± 0.08	4
Δ(1−5)	-----LSASDLA-	81.9 ± 0.5	90.7 ± 10.9	7.5	0.38 ± 0.09	44 ± 1	120 000
Δ(6−10)	SSLIL-----LA-	73.3 ± 2.3	60.0 ± 3.4	4.8	ni[b]	ni	ni
Δ(1−10)	----------LA-	67.9 ± 0.9	53.5 ± 8.9	4.6	ni	ni	ni
$(Gly)_5$	SSLIL**GGGGG**LA-	73.1 ± 1.1	66.9 ± 6.0	6.0	290 ± 50	126 ± 13	432
$(Pro)_5$	SSLIL**PPPPP**LA-	72.2 ± 0.3	61.1 ± 2.7	5.6	130 ± 30	26.9 ± 1.8	205
wt	reduced	63.8 ± 0.9	58.6 ± 6.9	3.8	nd[c]	nd	nd
A8P	SSLILLS**P**SDLA-	81.1 ± 1.5	74.6 ± 2.6	7.0	310 ± 27	21 ± 5	68
D10A	SSLILLSAS**A**LA-	81.5 ± 0.4	84.5 ±5.7	6.5	440 ± 160	0.17 ± 0.06	0.4
D10P	SSLILLSAS**P**LA-	76.0 ± 1.4	72.2 ± 5.0	6.7	350 ± 15	2.8 ± 0.4	8
W15F	SSLILLSASDLAGQ**F**-	76.8 ± 1.8	52.3 ± 3.7	4.9	340 ± 30	2.0 ± 0.3	6

[a] Helical residues are underlined and mutations are in boldface type. ΔG_u is the Gibbs free energy of unfolding at 25 °C determined by extrapolation to [GdmCl] = 0. Values are given as mean ± standard deviation of at least three independent determinations for all values except those for ΔG_u, which are the average of two or three experiments. The estimated uncertainty in ΔG_u is less than ±10%. Kinetic and dissociation constants for the first six entries are from ref *13*. K_D values were calculated from the ratio k_{off}/k_{on} as described in ref *13*. [b] ni, = no inhibition. [c] nd, not determined.

the figure, T_m = 82.35 ± 0.05 °C and ΔH_m = 86.5 ± 0.8 kcal mol^{-1} for wt APRin compared to 70.0 ± 0.5 °C and 42.1 ± 2.7 kcal mol^{-1} for the Δ(1−10) mutant. The values estimated in this set of experiments are within the uncertainty associated with replicate measurements determined with eq 3 and shown in Table 2.

To explore the mechanism of N-terminal thermal stabilization of APRin, we determined the melting behavior of proteins with smaller deletions as well as single-amino acid substitutions expected to destabilize the helix. The results of these experiments are summarized in Table 2. The data show that deletion of the five N-terminal residues Ser-Ser-Leu-Ile-Leu- did not significantly alter thermal stability, whereas deletion of residues 6−10 (-Leu-Ser-Ala-Ser-Asp-) resulted in a decrease in T_m of ∼8 °C. Substitution of five helix-breaking Gly or Pro residues at positions 6−10 also decreased T_m by 8 and 9 °C, respectively. These results suggest that the conformational state of residues 6−10 strongly influences the thermal stability of APRin.

Figure 1 and Table 1 show that residues 6−10 are involved in hydrogen-bonding interactions that would be expected to stabilize helix A. We therefore constructed the following single amino acid mutants of these positions to assess their role in APRin folding stability. Ala8 is located at the N-terminus of helix A where its carbonyl group serves as a hydrogen-bond acceptor for the peptide -NH of Leu11 and Ala12. Because both of these interactions could be retained in an Ala8Pro mutant, this mutation should have little effect on stability. The Asp10Ala and Asp10Pro mutations should disrupt hydrogen bonds involving the carboxyl group of Asp; in addition, the Pro10 would be unable to serve as a hydrogen-bond donor. Finally, the Trp15Phe mutation will result in the loss of the hydrogen bond from NHϵ1 to the carbonyl of Leu11; this mutation not only would destabilize helix A but also could allow enhanced accessibility of solvent to the interior of the barrel by destabilizing packing of the indole group into the top of the barrel.

In the series of single amino acid substitutions outlined above, the greatest effect on thermal stability was found with the Asp10Pro and Trp15Phe mutants, both of which exhibited decreased T_m values of ∼5 °C. The Trp15Phe mutant also showed a relatively large decrease in ΔH_m of ∼24 kcal mol^{-1} (Table 2), suggesting a significant decrease in noncovalent

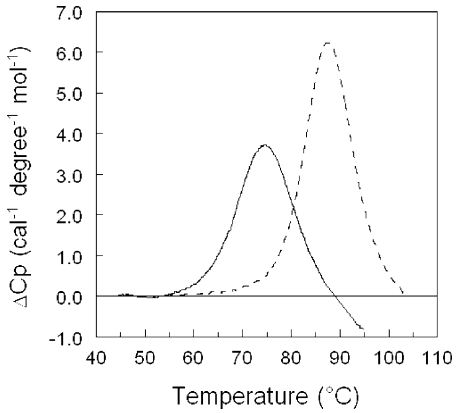

FIGURE 3: Changes in excess heat capacity measured by differential scanning calorimetry of wt APRin (---) and Δ(1−10) APRin (—). T_m values estimated from the peak in the curves were 86.8 and 73.8 °C for wt and Δ(1−10) APRins, respectively. In a rescan of the cooled solutions, approximately 60% and 80% of heat change was recovered for the wt and truncated mutants.

stabilizing interactions, possibly brought about by a loosening of the internal structure of the barrel. The Ala8Pro and Asp10Ala mutants were essentially unchanged in T_m and ΔH_m compared to the wt protein. The lack of an effect of changing Asp10 to Ala (which would delete the Asp10 carboxyl−Ser7 hydroxyl hydrogen bond) suggests either that this interaction does not occur in the wild-type protein, that it contributes negligibly to stability, or that a new, compensating interaction develops in the mutant. The absence of an effect of the Ala8Pro mutation was expected because, as indicated above, the stabilizing interactions involving this residue could be retained in the mutant protein.

Thermal Unfolding by DSC. DSC experiments were carried out with wt APRin and the Δ(1−10) mutant to confirm that the N-terminal trunk confers global folding stability on APRin. We also expected to obtain calorimetric values for enthalpy and heat capacity changes that could be used to estimate the room-temperature free energy of unfolding. The resulting thermograms are shown in Figure 3. The maxima in the melting profiles allow estimation of T_m values, which were 87.5 and 74.6 °C for the wt and Δ(1−10) proteins, respectively. Thus, the DSC data confirm that the 10 N-terminal residues of APRin impart significant thermal global stability to APRin. However, it was not possible to

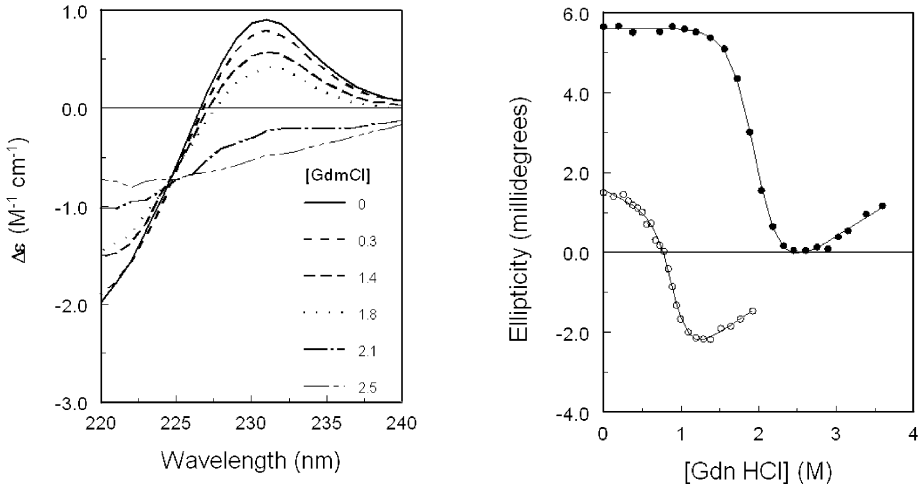

FIGURE 4: Denaturation of wt APRin by GdmCl assessed by CD. The left panel shows spectra obtained when wt APRin (6 μM in 50 mM Tris-HCl, pH 7.36) was titrated with 8.0 M GdmCl in the same buffer. The data were corrected for dilution. Final denaturant concentrations associated with each spectrum are shown in the figure. The right panel shows GdmCl denaturation profiles for wt APRin (6 μM, ●) and Δ(1−10) APRin (4 μM, ○). The lines were calculated from eq 6 using the best fitting values of the adjustable parameters, which for wt APRin were $\Delta G_u = 7150 \pm 300$ cal/mol and $m = 3655 \pm 154$ cal mol^{-1} M^{-1}. For Δ(1−10) APRin, $\Delta G_u = 4660 \pm 450$ cal/mol and $m = 5135 \pm 480$ cal mol^{-1} M^{-1}.

determine accurately ΔH or ΔC_p because the high-temperature baseline for unfolding was obscured by exothermic event(s) that probably were related to the formation of the irreversibly unfolded protein species seen in the CD experiments.

An unexpected result of the calorimetric experiments was that the T_m values found were ∼5 °C higher than those obtained from CD measurements, a difference that exceeds the uncertainty in determining the temperature in either method. This discrepancy in apparent T_m did not result from differences conditions used in the two types of experiment as the T_m values measured by CD were the same at protein concentrations of 5 or 100 μM and did not change when the rate of heating was increased (data not shown). In addition, the T_m values obtained by DSC were the same when the sample was heated more slowly (20 °C/h). It seems likely that the differences in apparent T_m resulted from monitoring different aspects of the unfolding process by the two techniques. DSC reflects global changes in interactions accompanying the unfolding processes, whereas the 230-nm CD signal, to which Trp15 contributes about a third, may be more sensitive to tertiary structure at the top of the barrel that may precede global unfolding.

Thermal Stability of Disulfide-Reduced APRin. Disulfide bonds are well-known to stabilize the folded state of proteins through their effect of decreasing the configurational entropy of the unfolded state relative to the folded state (*27*). The room-temperature CD spectra of the native and DTT-treated wt protein were essentially identical (data not shown), suggesting that reduction of the disulfide bond Cys26−Cys49 did not change its tertiary or secondary structure at these temperatures; the reduced protein did exhibit a decrease in T_m of ∼18 °C and a decrease in ΔH_m of ∼25 kcal mol^{-1}.

GdmCl-Induced Unfolding. A goal of this study was to determine the effect of the N-terminal residues on the thermodynamic stability ΔG_u of the protein at physiological temperatures. Because of the differences between the CD and calorimetric T_m values noted above, as well as the inability to estimate ΔC_p of unfolding calorimetrically, we turned to chemical denaturation as a means of comparing the room-temperature thermodynamic stability of the various APRin derivatives.

GdmCl-induced unfolding was followed by monitoring changes in the CD spectrum. The left panel of Figure 4 shows a series of CD spectra of wt APRin determined at various concentrations of GdmCl from 0 to 2.5 M. As with the thermal denaturation spectra, the largest difference in ellipticity was near 230 nm, but the isodichroic point was near 225 nm rather than 220 nm as observed in thermal denaturation. CD data similar to those shown in the left panel of Figure 4 were used to construct GdmCl denaturation profiles of wt and Δ(1−10) APR shown in the right panel of Figure 4. Optimized values of ΔG_u for these two experiments were estimated by fitting the data points in Figure 4 to eq 6. The resulting values of ΔG_u were 7150 ± 300 cal/mol for the wt protein and 4660 ± 450 cal/mol for Δ(1−10) APRin; the corresponding m values were 3655 ± 154 and 5135 ± 480 cal mol^{-1} M^{-1}, respectively. From the ratio $\Delta G_u/m$, $[GdmCl]_{1/2}$, the midpoint GdmCl concentration for denaturation, was estimated to be 2.0 M for wt APRin and 0.9 M for Δ(1−10) APRin. ΔG_u values determined from similar titrations for all of the APRin derivatives in the study are summarized in Table 2.

Comparison of APRin Stability Parameters. Changes in T_m and $[GdmCl]_{1/2}$ for the APRin mutants relative to the wt protein are summarized in the upper panel of Figure 5. The order of thermal stability as assessed by T_m is wt ≈ Δ(1−5) ≈ Ala8Pro ≈ Asp10Ala > Asp10Pro > Trp15Phe ≈ Δ(6−10) > Gly^{6-10} > Pro^{6-10} > Δ(1−10) > DTT-reduced APRin. The changes in $[GdmCl]_{1/2}$ generally paralleled those of T_m; that is, a decrease in T_m was accompanied by a decrease in sensitivity to GdmCl. The effects of these mutations on ΔG_u are also summarized in the bottom panel of Figure 5, which shows that deletion of residues 1−10 or 6−10 decreased ΔG_u by ∼2−3 kcal mol^{-1}, while substitution of residues 6−10 with a $(Gly)_5$ or $(Pro)_5$ linker decreased ΔG_u by ∼1−2 kcal mol^{-1}. Substitution of Trp15 by Phe reduced ΔG_u by slightly less than 3 kcal mol^{-1}, whereas reduction of the disulfide bond destabilized by a similar amount (3.5 kcal mol^{-1}).

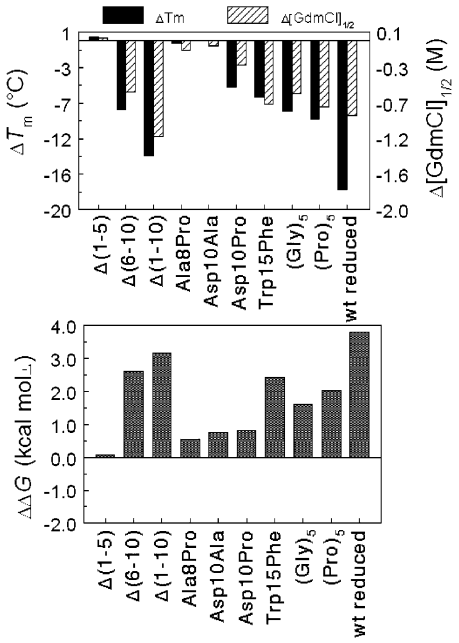

FIGURE 5: Summary of melting temperatures, susceptibilities to GdmCl-induced unfolding, and thermodynamic stabilities of APRin derivatives relative to wt APRin. Top panel: Changes in T_m generally correlate with changes in midpoint concentration of GdmCl required for unfolding. Bottom panel: $\Delta\Delta G_u$ values for wt and mutant APRins assessed from GdmCl denaturation curves. $\Delta\Delta G = \Delta G_u$ of wt $- \Delta G_u$ of mutant. A positive value of $\Delta\Delta G$ means that the mutant protein is less stable than the wild-type protein. ΔG_u values were generated from data similar to that shown in Figure 4 by curve-fitting with the method of Pace and Shaw (*22*).

Inhibitory Properties of Mutant APRins. Our previous experiments showed that APRin and the truncation mutants in this paper bind to APR in a simple bimolecular association reaction (*13*). The association and dissociation rates constants (k_{on} and k_{off}), and the apparent K_D derived from the ratio k_{off}:k_{on} were calculated for the new inhibitors by methods previously validated for the wt and truncation mutants (*13*). The kinetic and calculated equilibrium dissociation constants are summarized in Table 2. The rate constants for APRin association with APR were approximately the same for all the full-length mutant proteins prepared for this study as that previously observed for wt APRin. However, the dissociation rate constants for some of the new mutants were significantly different from those of the wt protein. For example, k_{off} for the Ala8Pro mutant was increased by about 20-fold compared to wt APRin, while that for the Asp10Pro mutant was about twice as fast as wt APRin. For the Asp10Ala mutant, k_{off} decreased by about 10-fold compared to the wt protein. These results suggest that the conformational properties of helix A influence the stability of the APR−APRin complex, largely by determining the rate of dissociation of the inhibitor from the complex.

Molecular Dynamics Simulation of wt APRin. Because a structure of the free inhibitor was not available when this study was initiated, we undertook a molecular dynamics simulation to determine if helix A would be maintained in a simulation of the solvated protein carried out by molecular dynamics under physiological conditions. Molecular dynamics simulations have been used previously to model helical transitions (see Discussion and refs *28*−*30*). The resulting model of the free inhibitor after 1.5 ns of simulation is shown in the right illustration in panel A of Figure 6. For comparison, the X-ray structure of the inhibitor in its complex with APR is shown in the left illustration in panel A. It is evident that the β-barrel topology and helix A are preserved in the model of the solvated, free inhibitor. In addition, except for the loop connecting β-strands I and II, the positions of the other loops connecting the β-strands were maintained. The congruence of the backbone of the free and bound inhibitors is illustrated in panel B of Figure 6, in which the Cα trace of the free inhibitor (magenta ribbon) has been superimposed on that of the APR-bound inhibitor (blue ribbon). In this figure, the Cαs of residues 6−105 were superimposed by a least-squares procedure by use of software in the Insight II modeling program. The root-mean-square deviation of the fit was 1.18 Å, reflecting the high degree of overlap of the two structures. As noted in the Introduction, our NMR structural data confirm that the secondary structural features, in particular the presence of helix A, are preserved in the unbound inhibitor in solution (*15*).

DISCUSSION

The two major conclusions of this study are first, that helix A of the N-terminal trunk of the serralysin inhibitor APRin of *P. aeruginosa* is an important determinant of the thermodynamic stability of the protein, and second, it influences the binding affinity of APRin for APR even though it makes no direct contact with the enzyme. The most pronounced

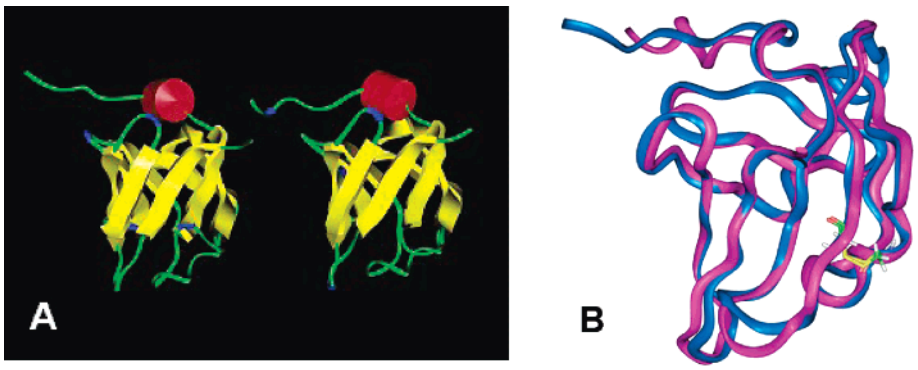

FIGURE 6: (A) Ribbon diagrams comparing the secondary structural elements and folding topography of APRin in its complex with APR as determined by X-ray crystallography (*11*) (left illustration) and as modeled by molecular dynamics (right illustration). β-Strands are depicted as yellow arrows, α-helices as red cylinders, turns in blue, and unordered structures in green. (B) α-Carbon overlay of APRin in its complex with APR (blue ribbon) with the modeled structure of the free inhibitor (magenta ribbon). The disulfide bond Cys26−Cys49 is depicted in stick format (lower right) and colored by atom type.

effect on APRin stability was brought about by deletion of 10 N-terminal amino acids of APRin, which lowered its melting temperature by ~13 °C as assessed both by CD and by DSC measurements. By comparison, reduction of the disulfide bond of the protein, a modification that generally results in destabilization of proteins, decreased the melting temperature by only ~5 °C more than deletion of residues 1−10.

GdmCl denaturation experiments allowed estimation of the intrinsic thermodynamic stability of the folded protein, which, at a value of ~7 kcal mol^{-1} at room temperature, is commensurate with the stability of many single-domain, globular proteins. Of the N-truncated APRins in this study, all except Δ(1−5) exhibited a decrease in conformational stability as assessed by ΔG_u extrapolated from GdmCl denaturation curves. The stability of Δ(1−5) APRin was essentially the same as that of the wt protein.

On the basis of accepted models of protein stability (*19*, *31*), the relatively large effect of the N-terminal trunk on the stability of APRin was surprising. Extensive studies of Matthews and co-workers on the thermal stability of T4 lysozyme have shown that surface residues generally contribute little to global protein stability because they are nearly equally solvated in the folded and unfolded states (*31*). In T4 lysozyme, alteration of solvent-exposed residues generally had a negligible effect on stability, with destabilizing mutations confined to regions of low solvent accessibility and high rigidity as assessed by crystallographic *B*-factors (*31*). Because of its surface location in free APRin as indicated by modeling, the trunk should be about equally solvated in the folded and unfolded states of the inhibitor and therefore, for the reasons cited above, should contribute minimally to APRin stability. Indeed, this was the case with the five N-terminal residues, whose deletion had no effect on either T_m or ΔG_u.

In looking for a reasonable structural explanation for the effect of the N-terminal trunk on the stability of APRin, we noted that the critical residues conferring temperature sensitivity are involved in helix A, a structure that is present in the crystal structures of the complex of two different APRin inhibitors with two different serralysins. As shown in Figure 1, which depicts the APR−APRin complex, the trunk is connected to the β-barrel by helix A. Our NMR data show that free APRin retains helix A (*15*), and the molecular dynamics simulation reported here is also consistent with this conclusion. Similar molecular dynamics simulations have been used previously to model helix transitions. For example, Wriggers et al. (*29*), starting with a crystal structure of calmodulin, carried out a simulation of this protein in explicit solvent at physiological ionic strength and temperature using protocols similar to those utilized here. They reported that, during the first 1.5 ns of the simulation, extensive unwinding of the calmodulin central α-helix was observed, a process that mimics the unwinding of the helix that is thought to occur on interaction with calmodulin-binding proteins. The energy of the system stabilized after about 2 ns of simulation and remained stable for the remaining 1 ns of the trajectory, a time period similar to that used in our simulation of solvated APRin.

The effect of modification of the trunk region on the stability of APRin is a specific effect related to the peptide segment comprising residues 6−10 rather than a nonspecific effect related to the length of the trunk, since deletion of residues 1−5 had no effect on APRin stability. The T_m and ΔG_u of the Asp10Ala and Ala8Pro mutants were also the same as for the wt protein, an observation that is consistent with the helix-stabilizing effect of Ala compared to Asp, as well as the well-known ability of Pro to function at the N-terminus of a helix (*32*, *33*).

The structural basis underlying the effect of helix A on the stability of APRin is most likely that the helix stabilizes a "cap" to the barrel. This structure, consisting largely of Trp15, may prevent access of solvent to the interior of the barrel, which is tightly packed with nonpolar residues (*11*). Assuming that the barrel retains the structure of the wt inhibitor when trunk residues 1−10 are removed [which is supported by the similar CD spectra of the two proteins (*13*)], we estimated [by the method of Fraczkiewicz and Braun (*34*, *35*) with a 1.4 Å probe] that removing residues 1−10 would expose about 340 $Å^2$ surface area to water. The residues exhibiting the greatest change in exposure were Leu11, Ala12, Asp32, Pro63, and Pro65, with Tyr41 and Thr64 experiencing a lesser degree of exposure. Leu11, which would become the new N-terminus in such a deletion mutant, is involved in a hydrogen bond through its carbonyl to Trp15Nε. The resulting increased accessibility of water could disrupt this interaction, possibly resulting in enhanced access of solvent to the interior and increased flexibility of Trp15, even though Trp 15 itself may not become more exposed upon deletion of the 10 trunk residues. In a similar fashion for the other mutants, destabilizing helix A could allow increased access of solvent to the interior of the barrel, thereby decreasing the global stability of the folded protein.

A similar example of the effect of a capping helix on the stability of a β-barrel is provided by the recent study of Shehi et al. (*36*) on the DNA binding protein Sso7d of the thermophile *Sulfolobus solfataricus*. These authors reported that removal of eight C-terminal residues from this 67-residue protein decreased T_m from 98 to 52 °C with a concomitant decrease in ΔH_m of ~35 kcal mol^{-1}. The β-barrel structure of Sso7d is capped by an eight-residue C-terminal helix; evidently, when this helix is removed, a much less stable protein is produced. As the authors pointed out, removal of the helix would be expected to expose the hydrophobic core of the barrel to aqueous solvent, thereby destabilizing it.

The kinetic data presented here as well as our prior studies suggest that helix A also influences enzyme−inhibitor affinity. Previously, we showed that deletion of successive residues from the trunk of APRin resulted in progressively increased values of K_D (*13*). The effect of trunk length on apparent binding affinity is consistent with cystallographic data showing that the N-terminal region of the inhibitor occupies part of the substrate binding site of the enzyme, with the extent of penetration limited by the body of β-barrel, one face of which packs against the proteinase surface near its Met turn region (*11*, *12*). With fewer contacts between the trunk and the enzyme in the truncation mutants, the affinity of the inhibitor for the enzyme should be reduced. However, an unexpected observation was that while APRin with residues 1−5 deleted retained the ability to inhibit APR, removal of the equivalent number of residues not in contact with the proteinase (residues 6−10) gave a noninhibitory protein (*13*). Replacement of residues 6−10 with either five Gly or five Pro residues restored inhibition but with a 100−200-fold reduction in affinity. In the present study, the single amino acid mutations involving helix A show that residues

at positions 6−10 influence the stability of the complex, primarily by affecting the dissociation rate of the inhibitor from the complex as opposed to the association rate. The Asp10Pro and Asp10Ala mutations exhibited increased rates of dissociation with an unaltered association rate. The Ala8Pro mutation, which is expected to have decreased conformational flexibility while possibly retaining a helical structure, exhibited a 10-fold reduction in dissociation rate. Taken together, these results suggest that helix A may reduce the conformational flexibility of the trunk, thereby decreasing the probability of dissociation of the complex by decreasing the entropy cost associated with the formation of a more flexible trunk in the free inhibitor. Another possibility is that helix A could orient the barrel surface with respect to the trunk and thereby promote productive interaction between the barrel surface and its interaction site near the Met turn of APR.

In conclusion, our studies show that a conserved single-turn helix found in the serralysin inhibitor−proteinase complex strongly influences the global stability of the inhibitor protein. This helix, which does not interact directly with the proteinase, also plays a role in determining of the strength of interaction between the inhibitor and proteinase, largely by influencing the rate of enzyme−inhibitor dissociation.

REFERENCES

1. Maeda, H., and Morihara, K. (1995) Serralysin and related bacterial proteinases, *Methods Enzymol. 248*, 395−413.
2. Stöcker, W., Grams, F., Baumann, U., Reinemer, P., Gomis-Rüth, F. X., McKay, D. B., and Bode, W. (1995) The metzincins−topological and sequential relations between the astacins, adamalysins, serralysins, and matrixins (collagenases) define a superfamily of zinc-peptidases, *Protein Sci. 4*, 823−840.
3. Morihara, K. (1963) *Pseudomonas aeruginosa* proteinase. I. Purification and general properties, *Biochim. Biophys. Acta 73*, 113−124.
4. Horvat, R. T., and Parmely, M. J. (1988) *Pseudomonas aeruginosa* alkaline protease degrades human gamma interferon and inhibits its bioactivity, *Infect. Immun. 56*, 2925−2932.
5. Heck, L. W., Morihara, K., and Abrahamson, D. R. (1986) Degradation of soluble laminin and depletion of tissue-associated basement membrane laminin by *Pseudomonas aeruginosa* elastase and alkaline protease, *Infect. Immun. 54*, 149−153.
6. Twining, S. S., Kirschner, S. E., Mahnke, L. A., and Frank, D. W. (1993) Effect of *Pseudomonas aeruginosa* elastase, alkaline protease, and exotoxin A on corneal proteinases and proteins, *Invest. Ophthalmol. Vis. Sci. 34*, 2699−2712.
7. Matsumoto, K., Shams, N. B., Hanninen, L. A., and Kenyon, K. R. (1992) Proteolytic activation of corneal matrix metalloproteinase by *Pseudomonas aeruginosa* elastase, *Curr. Eye Res. 11*, 1105−1109.
8. Okamoto, T., Akaike, T., Suga, M., Tanase, S., Horie, H., Miyajima, S., Ando, M., Ichinose, Y., and Maeda, H. (1997) Activation of human matrix metalloproteinases by various bacterial proteinases, *J. Biol. Chem. 272*, 6059−6066.
9. Molla, A., Yamamoto, T., Akaike, T., Miyoshi, S., and Maeda, H. (1989) Activation of Hageman Factor and prekallikrein and generation of kinin by various microbial proteinases, *J. Biol. Chem. 264*, 10589−10594.
10. Létoffé, S., Delepelaire, P., and Wandersman, C. (1989) Characterization of a protein inhibitor of extracellular proteases produced by *Erwinia chrysanthemi*, *Mol. Microbiol. 3*, 79−86.
11. Hege, T., Feltzer, R. E., Gray, R. D., and Baumann, U. (2001) Crystal structure of a complex between *Pseudomonas aeruginosa* alkaline protease and its cognate inhibitor. Inhibition by a zinc−NH_2 coordinative bond, *J. Biol. Chem. 276*, 35087−35092.
12. Baumann, U., Bauer, M., Létoffé, S., Delepelaire, P., and Wandersman, C. (1995) Crystal structure of a complex between *Serratia marcescens* metallo-protease and an inhibitor from *Erwinia chrysanthemi*, *J. Mol. Biol. 248*, 653−661.
13. Feltzer, R. E., Gray, R. D., Dean, W. L., and Pierce, W. M., Jr. (2000) Alkaline proteinase inhibitor of *Pseudomonas aeruginosa*. Interaction of native and N-terminally truncated inhibitor proteins with *Pseudomonas* metalloproteinases, *J. Biol. Chem. 275*, 21002−21007.
14. Feltzer, R. E., Trent, J. O., and Gray, R. D. (2003) Alkaline proteinase inhibitor of *Pseudomonas aeruginosa*: A mutational and molecular dynamics study of the role of N-terminal residues in the inhibition of *Pseudomonas* alkaline proteinase, *J. Biol. Chem. 278*, 25952−25957.
15. Arumugam, S., Gray, R. D., and Lane, A. N. ^{1}H, ^{15}N and ^{13}C assignments of the alkaline proteinase inhibitor APRin from *Pseudomonas aeruginosa*. *J. Biomol. NMR*, in press.
16. Edsall, J. T., and Wyman, J. (1958) *Biophysical Chemistry*, Vol. I, p 455, Academic Press, New York.
17. Lumry, R., and Biltonen, R. (1966) Validity of the "two-state" hypothesis for conformational transitions of proteins, *Biopolymers 4*, 917−944.
18. Privalov, P. I. (1979) Stability of Proteins, *Adv. Protein Chem. 33*, 167−241.
19. Dill, K. A., and Shortle, D. (1991) Denatured states of proteins, *Annu. Rev. Biochem 60*, 795−825.
20. John, D. M., and Weeks, K. M. (2000) van't Hoff enthalpies without baselines, *Protein Sci. 9*, 1416−1419.
21. Knapp, S., Karshikoff, A., Berndt, K. D., Christova, P., Atanasov, B., and Ladenstein, R. (1996) Thermal unfolding of the DNA-binding protein Sso7d from the hyperthermophile *Sulfolobus solfataricus*, *J. Mol. Biol. 264*, 1132−1144.
22. Pace, C. N. and Shaw, K. L. (2000) Linear extrapolation method of analyzing solvent denaturation curves, *Proteins: Struct., Funct., Genet.* (*Suppl.) 4*, 1−7.
23. Santoro, M. M. and Bolen, D. W. (1988) Unfolding free energy changes determined by the linear extrapolation method. 1. Unfolding of phenylmethanesulfonyl α-chymotrypsin using different denaturants, *Biochemistry 27*, 8063−8068.
24. Weingarten, H. and Feder, J. (1986) Cleavage site specificity of vertebrate collagenases, *Biochem. Biophys. Res. Commun. 139*, 1184−1187.
25. Trent, J. O. (2001) Molecular modeling of drug−DNA complexes: an update, *Methods Enzymol. 340*, 290−326.
26. Woody, R. W. (1994) Contributions of tryptophan side chains to the far-ultraviolet circular dichroism of proteins, *Eur. Biophys. J. 23*, 253−262.
27. Pace, C. N., Grimsley, G. R., Thomson, J. A., and Barnett, B. J. (1988) Conformational stability and activity of ribonuclease T1 with zero, one, and two intact disulfide bonds, *J. Biol. Chem. 263*, 11820−11825.
28. Gray, T. M., Arnoys, E. J., Blankespoor, S., Born, T., Jagar, R., Everman, R., Plowman, D., Stair, A., and Zhang, D. (1996) Destabilizing effect of proline substitutions in two helical regions of T4 lysozyme: Leucine 66 to proline and leucine 91 to proline, *Protein Sci. 5*, 742−751.
29. Wriggers, W., Mehler, E., Pitici, F., Weinstein, H., and Schulten, K. (1998) Structure and dynamics of calmodulin in solution, *Biophys. J. 74*, 1622−1639.
30. Zhu, Y., Alonso, D. O. V., Maki, K., Huang, C.-Y., Lahr, S. J., Daggett, V., Roder, H., DeGrado, W. F., and Gai, F. (2003) Ultrafast folding of α3D: A de novo designed three-helix bundle protein, *Proc. Natl. Acad. Sci. U.S.A. 100*, 15486−15491.
31. Matthews, B. W. (1993) Structural and genetic analysis of protein stability, *Annu. Rev. Biochem. 62*, 139−160.
32. O'Neil, K. T., and DeGrado, W. F. (1990) A thermodynamic scale for the helix-forming tendencies of the commonly occurring amino acids, *Science 250*, 646−651.
33. Blaber, M., Zhang, X. J., Lindstrom, J. D., Pepiot, S. D., Baase, W. A., and Matthews, B. W. (1994) Determination of alpha-helix propensity within the context of a folded protein. Sites 44 and 131 in bacteriophage T4 lysozyme, *J. Mol. Biol. 235*, 600−624.
34. Fraczkiewicz, R. and Braun, W. (1998) Exact and efficient analytical calculation of the accessible surface areas and their gradients for macromolecules, *J. Comput. Chem. 19*, 319−222.
35. http://www.scsb.utmb.edu/cgi-bin/get_a_form.tcl.
36. Shehi, E., Granata, V., Del Vecchio, P., Barone, G., Fusi, P., Tortora, P., and Graziano, G. (2003) Thermal stability and DNA binding activity of a variant form of the Sso7d protein from the archeon *Sulfolobus solfataricus* truncated at leucine 54, *Biochemistry 42*, 8362−8368.

BI048287Q